Chemical Physics 71 (1982) 401–415
North-Holland Publishing Company

AVOIDED-CROSSING MOLECULAR-BEAM SPECTROSCOPY OF CH_3SiF_3

W. Leo MEERTS
Fysisch Laboratorium, Katholieke Universiteit, Toernooiveld, 6525 ED Nijmegen, The Netherlands

and

Irving OZIER
Department of Physics, University of British Columbia, 6224 Agriculture Road, Vancouver, V6T 2A6 Canada

Received 18 March 1982

The avoided-crossing molecular-beam method has been applied to CH_3SiF_3 in the ground torsional state. Stark and hyperfine rotational anticrossings have been studied, along with barrier anticrossings in which the zero-field energy differences depend only on the *torsional* splittings. For $v = 0$, pure rotational spectra were measured for $J = 13 \leftarrow 12$ and $14 \leftarrow 13$ with a mm-wave spectrometer and for $J = 1 \leftarrow 0$ with the molecular-beam spectrometer. Stark and Zeeman studies have been carried out with conventional beam techniques. From a simultaneous analysis of existing microwave data for $v \geq 2$ and the current measurements, it was found that the moment of inertia of the methyl top $I_\alpha = 3.170(2)$ amu Å^2, the effective rotational constant $A^{\text{eff}} = 4059.522(22)$ MHz, and the effective height of the barrier $V_3^{\text{eff}} = 413.979(14)$ cm^{-1}. The true values of A and V_3 have been obtained within certain approximations. The rotational constant B and several distortion constants including D_K were evaluated. In addition to determining the electric dipole moment μ to be 2.33938(14) D, the data yielded values for the distortion dipole constants μ_D and μ_J, and the molecular g-factors $g_\parallel$ and $g_\perp$.

1. Introduction

A significant advance in the study of internal rotation of symmetric rotors has been made recently with the development of the avoided-crossing molecular-beam method [1,2]. In favourable cases, this technique allows the determination of energy separations Δ_0 between levels that are not connected by a matrix element of the permanent dipole moment. The $(\Delta K = 0)$ selection rule can be overcome in this way, so that the leading terms in the torsion–rotation hamiltonian can now be measured directly.

The avoided crossings can be classified according to the mechanism which provides the mixing between the interacting levels [2–4]. In the "Stark anticrossings", this mixing arises from the centrifugal distortion dipole moment μ_D [5,6]. The selection rules are $\Delta K = \pm 3$ and $\Delta\sigma = 0$ [2], where $\sigma = -1, 0, +1$ labels the torsional sublevels. In the "hyperfine anticrossings", the mixing is produced by the nuclear hyperfine effects. Here the selection rules are $\Delta K = 0, \pm 1, \pm 2$, depending on the specific hyperfine operator involved, and $\Delta\sigma = 0, \pm 1$ [2].

The avoided crossings can also be classified according to the physical origin of the zero-field energy separation Δ_0. If this contains a contribution from the energy of rigid rotation, the anticrossing is referred to as "rotational". If Δ_0 arises entirely from torsional terms, we have a "barrier" anticrossing. In both cases, to lowest order, the crossing field ϵ_c at which the two interacting levels have their minimum separations ν_m is proportional to the ratio of Δ_0 to the electric dipole moment μ.

In the initial experiment [2], a series of $(\Delta J = 0)$ rotational anticrossings were studied in CH_3CF_3. Of the Stark cases measured, all involved $K = \pm 2 \leftrightarrow \mp 1$, because this type has the lowest ϵ_c [3]. In the most recent work [4], a series of barrier anticrossings were studied in CH_3SiH_3, along with a set of rotational avoided crossings [‡] between upper level $(J_\alpha = 1, K_\alpha = \pm 1, \sigma_\alpha)$ and lower level $(J_\beta = 2, K_\beta = 0, \sigma_\beta)$. No

[‡] As in the convention defined in ref. [3], the levels are labelled by the quantum numbers appropriate to the electric field range $0 \ll \epsilon \ll \epsilon_c$. For this field range, the upper and lower levels are denoted α and β, respectively.

0301-0104/82/0000–0000/$ 02.75

($\Delta J = 0$) rotational anticrossings were observed because the ϵ_c involved were too high.

A test of the current model for internal rotation in symmetric rotors was completed recently [7] using CH_3SiH_3 by analysing both the avoided-crossing data [4] and microwave measurements; the latter included older spectra [8] and extensive new results [7]. Because of cooling in the nozzle beam source, the anticrossing experiments were confined to the ground torsional level ($v = 0$); this is true of all the work to date including that reported here. The microwave experiments are based on the torsional satellite method introduced by Kivelson [9]; these measurements are made primarily in the excited torsional levels, but are much less sensitive to the leading terms in the hamiltonian. It was concluded that the model [7,10–12] works well for levels well below the top of the barrier, but breaks down for levels near the barrier top or above it [1].

In the current work, the avoided-crossing method has been applied to methyltrifluorosilane (CH_3SiF_3). With its internal rotor splittings in the 10 to 300 MHz range, its small difference ($A - B$) in rotational constants, and its large electric dipole moment μ, this molecule is very well suited to the study of both barrier and ($\Delta J = 0$) rotational anticrossings. A large number of both types have been observed, including Stark rotational anticrossings with $K = \pm 3 \leftrightarrow 0$. These had been predicted [3], but not previously detected. With absolute measurements of 21 different Δ_0 and 6 relative measurements, the internal consistency of the rotational and barrier experiments has been established to a high degree of accuracy.

A simultaneous analysis was carried out of both these beam data and the microwave spectra. The latter consisted of the existing cm-wave data [13] for $v \leqslant 3$ supplemented with current results from two ground-state studies: mm-wave measurements for $J = 13 \leftarrow 12$ and $J = 14 \leftarrow 13$, and molecular-beam electric-resonance (MBER) measurements for $J = 1 \leftarrow 0$. The analysis confirms the conclusion reached for methylsilane [7]. The established model for internal rotation [7,10–12] reproduced the frequencies for levels below the barrier top ($v \leqslant 2$), but the resulting least-squares parameters, as given in table 1, predict microwave frequencies for the levels near the barrier top ($v = 3$) that clearly disagree with experiment. It is not known whether the mechanism for the breakdown is a direct result of the levels' position with respect to the barrier top or is a result of an unrelated process, such as perturbation by a low-lying vibrational fundamental. However, with a second molecule now behaving in the same manner as CH_3SiH_3, it is becoming clear that the mechanism at work is intrinsic to the torsion–rotation–vibration hamiltonian.

In addition to this torsion–rotation investigation, a Stark–Zeeman study was carried out. The precision value of μ obtained was essential to the analysis of the anticrossing data. All the dipole constants and g-factors determined are listed in table 1.

Table 1
Molecular constants for CH_3SiF_3 [a]

Quantity	
μ/μ (OCS) [b]	3.270994(35)
μ(D) [b]	2.33938(14) [c,d]
$\mu_J(\mu D)$	1.23(26)
$\mu_D(\mu D)$	2.13(57)
$g_\parallel$(nm)	−0.0252(4)
$g_\perp$(nm)	−0.0178(2)
A^{eff}(MHz)	4059.521(21)
B (MHz)	3718.042(21) [d]
D_J (kHz)	0.8566(68)
D_{JK} (kHz)	2.521(11)
D_K (kHz)	−4.32(33)
ρ	0.02546055(48)
V_3^{eff} (cm^{-1})	413.994(9) [d]
F_{3J} (MHz)	−18.91(12) [d]
F_{9J} (MHz)	−0.524(58)
D_{Jm} (MHz)	0.0906(27) [d]
D_{Km}^{eff} (MHz)	0.208(40)

a) In evaluating the constants that enter H_{TR}, only the data with $v \leqslant 2$ were used.
b) Here μ represents $\mu_Q(3,2)$.
c) This was calculated using μ(OCS) = 0.71519(3) D [22].
d) Comparisons with previous values are given in the text.

2. Theory

The torsion–rotation hamiltonian H_{TR} for a sym-

metric rotor has received a great deal of attention over the years [10–12,14,15]. Most recently, H_{TR} has been discussed in the light of the development of the avoided-crossing method [4,7]. Here we shall only review very briefly the most important results following the notation of the earlier studies of CH_3SiH_3 [4,7,16].

In the internal-axis method (IAM),

$$H_{TR} = BJ^2 + (A - B)J_z^2 + Fp^2 + V_3[\tfrac{1}{2}(1 - \cos 3\alpha)] + H_D . \quad (1)$$

The first two terms result from rigid rotation, while the third and fourth arise from oscillations in the torsional angle α. H_D takes into account distortion effects associated with these two types of motion. In the limit that such effects are negligible, $F = A/\rho(1-\rho)$, where $\rho = I_\alpha/(I_\alpha + I_f)$. Here I_α and I_f are, respectively, the moments of inertia about the symmetry axis of the CH_3-top and the SiF_3-frame. In the current work, only the first term in the Fourier expansion of the hindering potential $V(\alpha)$ is retained because this leading term cannot be separated from the higher-order corrections [7]. If these corrections are negligible, then V_3 is the height of the potential barrier.

The distortion hamiltonian H_D can be expanded in terms of the square of the total angular momentum J, the component J_z of J along the symmetry axis z, the torsional angular momentum p, and the torsional operators $\frac{1}{2}(1 - \cos 3n\alpha)$, where n is an integer. If only the terms that enter directly into the analysis of the current data are retained, then

$$H_D = -D_J J^4 - D_{JK} J^2 J_z^2 - D_K J_z^4 - (D_{Jm} J^2 + D_{Km} J_z^2)p^2 + \tfrac{1}{2}(1 - \cos 3\alpha)(F_{3J} J^2 + F_{3K} J_z^2) + \tfrac{1}{2}(1 - \cos 9\alpha) F_{9J} J^2 . \quad (2)$$

The reason for including F_{9J} in preference to F_{6J} is discussed in section 8. Because various terms in H_D have been dropped, some of the constants in eqs. (1) and (2) must be interpreted as effective parameters [7]. For example, both F and ρ will deviate by small amounts from the definitions given above. A full discussion of H_D and the difficulties in separating the various parameters is given elsewhere [7].

The quantum numbers labelling the eigenvalues E_{TR} of H_{TR} are $(vJK\sigma m_J)$. The symmetry type of the torsional wavefunctions is A for $\sigma = 0$ and E for $\sigma = \pm 1$. The symmetry type Γ of the torsion–rotation wavefunctions is determined by the irreducible representation of group G_{18} corresponding to $(JK\sigma)$ [17]. m_J is the magnetic quantum number for the component of J along the space-fixed Z-direction, which is, of course, taken to be the direction of the external fields. When nuclear hyperfine effects are taken into account, several additional quantum numbers must be introduced. m_H and m_F are, respectively, the magnetic quantum numbers for the total hydrogen nuclear spin I_H and the total fluorine nuclear spin I_F. The eigenvalue of the Z-component of the total angular momentum is $m_T = m_J + m_H + m_F$.

In order to analyse the torsion–rotation data, E_{TR} was calculated as described in refs. [4,7] treating H_D with first-order perturbation theory. In order to determine the dipole moment μ in the Stark study and the zero-field splittings Δ_0 in the anticrossing experiments, the Stark–rotation hamiltonian was diagonalized [4,16] after truncation at $\Delta J = 3$. In this calculation, the rotational hamiltonian is treated as though $V_3 \to \infty$, but with B replaced by the $(v = 0)$ value of $\hat{B}$ as defined by eq. (6) below. For CH_3SiF_3, this value of $\hat{B}$ is 3715.658 MHz. The values of D_J and D_{JK} used are given in table 1. The fundamental constants were taken from Cohen and Taylor [18].

3. Experimental details

The experimental methods and conditions were very similar to those used for earlier studies of symmetric rotors [3,19,20]. The basic MBER apparatus has been described in detail elsewhere [21]. The very low rotational temperatures required were obtained using the seeded beam technique; a mixture of 4% CH_3SiF_3 in argon was expanded through a 40 μm nozzle at a backing pressure of 1.0 bar with the source at room temperature. The two strongest ion fragments SiF_3^+ and $CH_3SiF_2^+$ were detected simultaneously by adjusting the resolution of the mass spectrometer.

Three different C-field configurations were used. For the Stark–Zeeman studies, the large quartz C-field was employed [3] with a 120 mm long section coated for $(\Delta m_T = 0, \pm 1)$ transitions. For the anti-

crossings at relatively low field ($\epsilon_c \leq 2$ kV/cm), this same quartz field was used but with a 62 mm long section coated only for ($\Delta m_T = 0$) transitions [3]. For the high-field anticrossings, the small pyrex C-field was used with a 13 mm long section coated only for ($\Delta m_T = 0$) transitions [20]. A detailed discussion of the stability and calibration of the electric field has been given earlier [3,20].

4. The electric dipole moment

A precision measurement of the dipole moment was obtained by studying the usual MBER spectra $(J, \pm|K|, \mp|m_J|) \rightarrow (J, \pm|K|, \mp|m_J|+1)$. For the C-field used (see section 3), the full width $\Delta\nu_T$ at half height due to time of flight was ≈4 kHz. Preliminary observations were made of several spectra; each appeared as a structureless feature whose width was dominated by hyperfine and/or inhomogeneity effects. The final measurements of μ were made from the ($m_J = \mp 1 \rightarrow 0$) and ($\mp 2 \rightarrow \mp 1$) components for $J_K = 3_{\pm 2}$. At an electric field of ≈1226 V/cm, these fell at 240.0 and 238.6 MHz, respectively. For each component, the observed full width $\Delta\nu_{obs}$ at half height was ≈11 kHz and the signal-to-noise ratio was ≈2 for a time constant of 1 s. A signal-averager was used to obtain a signal-to-noise of at least 5/1. This specific J_K was chosen because, for this case, the frequencies measured for the components are independent [19] of the nuclear hyperfine effects and of the effective anisotropy $(\alpha_\parallel - \alpha_\perp)_{eff}$ in the polarizability. The latter takes into account [16] both the true anisotropy $(\alpha_\parallel - \alpha_\perp)$ and the J-dependence of the dipole moment that enters the second-order Stark effect.

The values of μ obtained for the two components agreed to 3 ppm, a difference consistent with the frequency error of ≈1 kHz. The ratio of the average to the dipole moment of OCS in the ($J = 1$) level of the ground vibrational state is given in table 1, along with the absolute value of μ calculated using $\mu(OCS) = 0.71519(3)$ [22]. This final value for CH_3SiF_3 agrees with the previous microwave determination [13] that $\mu = 2.33(10)$ D.

No attempt was made to study the rotational dependence of μ from these spectra. The effective dipole moment determined from such Stark measurements with $K \neq 0$ is given by [16,23]:

$$\mu_Q(J,K) = \mu_0 + \mu_J J(J+1) + \mu_K K^2 . \quad (3)$$

In the infinite barrier limit, μ_0 is the rotationless dipole moment in the ($v = 0$) level. For the current work, the only effect of internal rotation on eq. (3) is to change slightly the interpretation of the constant μ_0. See the appendix of ref. [16]. In eq. (3), μ_J and μ_K are distortion dipole constants. The number given for μ in table 1 actually represents μ_Q (3,2). From the value of μ_J in table 1, it is clear that the contribution of μ_J to μ_Q (3,2) is insignificant compared to the 140 ppm error in the absolute value of μ. The same conclusion is reached for μ_K if $|\mu_K/\mu_J| \lesssim 30$, which is a very generous upper limit. Even with relative measurements, it would be very difficult to obtain μ_J and/or μ_K from the conventional spectrum. However, relative measurements on the anticrossing spectra have been used find μ_J. See section 5.1.

5. The avoided crossing measurements

5.1. The Stark rotational anticrossings

Two series of Stark anticrossings with ($\Delta J = 0$) have been studied in CH_3SiF_3: one ‡ with $K = \pm 2 \leftrightarrow \mp 1$ for various σ and J, and the other with $K = \pm 3 \leftrightarrow 0$ for various σ but only $J = 3$. As shown in ref. [3], these two K-series are the only ones which meet the focusing requirements for transition detection in a conventional MBER spectrometer.

The various anticrossings searched for are listed in table 2. For each case which was not observed, the mixing matrix element η must be much smaller in magnitude than the typical values for the anticrossings detected. Our tentative conclusion is that the unobservable anticrossings are forbidden, i.e. the corresponding $\eta \equiv 0$. One selection rule which emerges clearly is $\Delta\sigma = 0$. Since the distortion dipole operator has no torsional part and does not break the rotational symmetry, one would expect the torsion–rotation symmetry to be conserved, i.e. $\Delta\Gamma = 0$. This implies directly $\Delta\sigma = 0$. A similar conclusion was reached earlier for CH_3CF_3 [2].

‡ In labelling an anticrossing, the first set of quantum numbers always refers to upper level α and the second set refers to lower level β.

Table 2
Summary of the selection rules investigated for anticrossings in CH_3SiF_3 [a]

J	Upper state				Lower state				Δm_J	Label [b]	Remarks [c]
	K_α	σ_α	Γ_α	m_J^α	K_β	σ_β	Γ_β	m_J^β			
2	± 2	0	E_1	± 1	∓ 1	0	E_1	± 1	0	SH	
2	± 2	∓ 1	E_2	± 1	∓ 1	∓ 1	E_2	± 1	0	SH	
2	± 2	± 1	E_3	± 1	∓ 1	± 1	E_3	± 1	0	SH	
2,3	± 2	0	E_1	± 2	∓ 1	0	E_1	± 2	0	S	
2,3	± 2	∓ 1	E_2	± 2	∓ 1	∓ 1	E_2	± 2	0	S	
2,3	± 2	± 1	E_3	± 2	∓ 1	± 1	E_3	± 2	0	S	
2	± 2	∓ 1	E_2	± 2	∓ 1	0	E_1	± 2	0	S	not observed
2	± 2	± 1	E_3	± 2	∓ 1	0	E_1	± 2	0	S	not observed
2	± 2	0	E_1	± 2	∓ 1	∓ 1	E_2	± 2	0	S	not observed
2	± 2	∓ 1	E_2	± 1	∓ 1	∓ 1	E_3	± 1	0	SH	not observed
2	± 2	± 1	E_3	± 1	∓ 1	∓ 1	E_2	± 1	0	SH	not observed
4	± 2	0	E_1	± 4	∓ 1	0	E_1	± 4	0	S	
5	± 2	± 1	E_3	± 1	∓ 1	± 1	E_3	± 1	0	SH	
5	± 2	0	E_1	± 5	∓ 1	0	E_1	± 5	0	S	
3	± 3	0	A_2	± 1	0	0	A_2	± 1	0	S	
3	± 3	∓ 1	E_4	± 1	0	∓ 1	E_4	± 1	0	S	
3	± 3	± 1	E_4	± 1	0	± 1	E_4	± 1	0	S	
2	± 2	0	E_1	± 2	0	0	A_1	0	± 2	H	
2	± 2	∓ 1	E_2	± 2	0	± 1	E_4	0	± 2	H	
2	± 2	∓ 1	E_2	± 2	0	0	A_1	0	± 2	H	$\Delta m_H = \mp 2$; $\Delta m_F = 0$
2	± 2	0	E_1	± 2	0	± 1	E_4	0	± 2	H	
2	± 2	± 1	E_3	± 2	0	± 1	E_4	0	± 2	H	not observed
2	± 2	± 1	E_3	± 2	0	0	A_1	0	± 2	H	not observed
2	± 2	0	E_1	± 2	0	0	A_1	± 1	± 1	H	
2	± 2	∓ 1	E_2	± 2	0	± 1	E_4	± 1	± 1	H	
2	± 2	∓ 1	E_2	± 2	0	0	A_1	± 1	± 1	H	
2	± 2	0	E_1	± 2	0	± 1	E_4	± 1	± 1	H	
1,2,3	± 1	∓ 1	E_3	± 1	∓ 1	0	E_1	± 1	0	EA	
1,2,3	± 1	± 1	E_2	± 1	∓ 1	0	E_1	± 1	0	EA	not observed
2	± 1	∓ 1	E_3	± 2	∓ 1	0	E_1	± 2	0	EA	
2	± 1	∓ 1	E_3	± 2	∓ 1	0	E_1	± 1	± 1	EA	$\Delta m_H = \mp 1$; $\Delta m_F = 0$

(continued on next page)

Table 2 *(continued)*

J	Upper state				Lower state				Δm_J	Label [b]	Remarks [c]
	K_α	σ_α	Γ_α	m_J^α	K_β	σ_β	Γ_β	m_J^β			
2	± 1	∓ 1	E_3	± 2	∓ 1	0	E_1	0	± 2	EA	not observed
2	± 1	± 1	E_2	± 2	∓ 1	0	E_1	± 2	0	EA	not observed
2	± 1	± 1	E_2	± 2	∓ 1	0	E_1	0	± 2	EA	not observed
2	± 2	∓ 1	E_2	± 1	± 2	0	E_1	∓ 1	± 2	EA	not observed
2	± 2	± 1	E_3	± 1	± 2	0	E_1	∓ 1	± 2	EA	not observed
3	± 1	∓ 1	E_3	± 2	∓ 1	0	E_1	± 2	0	EA	not observed
5	± 1	∓ 1	E_3	± 5	∓ 1	0	E_1	± 5	0	EA	
2	± 1	∓ 1	E_3	± 1	∓ 1	± 1	E_2	± 1	0	EE	
3	± 1	∓ 1	E_3	± 1	∓ 1	∓ 1	E_2	± 1	0	EE	
4	± 1	∓ 1	E_3	± 1	∓ 1	∓ 1	E_2	± 1	0	EE	
4	± 1	∓ 1	E_3	± 2	∓ 1	∓ 1	E_2	± 1	± 1	EE	

a) Upper signs go with upper and lower with lower.
b) For the Stark–hyperfine hybrids (SH), the selection rules listed refer only to the pure Stark component. See text.
c) Unless otherwise specified, the anticrossing was observed.

The selection rules for the magnetic quantum numbers follow [3] from the fact that the distortion dipole operator has no nuclear spin part. Clearly, $\Delta m_H = \Delta m_F = 0$. Since m_T must be conserved, Δm_J must also vanish. This argument does not apply to the hyperfine crossings; in this case, $\Delta m_J = 0, \pm 1, \pm 2$, depending on the specific operator involved.

Most anticrossings can be treated as a series of two-level problems; in the upper- and lower-state quantum numbers of table 2, as throughout the current work, upper signs go with upper and lower with lower (unless otherwise specified). However, the Stark–hyperfine hybrids listed in table 2 are exceptions. These are all of the type $(J, K = \pm 2, \sigma, m_J = \pm 1) \leftrightarrow (J, K = \mp 1, \sigma, m_J = \pm 1)$. The distortion dipole operator couples signs upper ↔ upper and lower ↔ lower with its ($\Delta K = \pm 3$, $\Delta m_J = 0$) matrix elements, while the magnetic dipole–dipole interaction can couple signs upper ↔ lower and lower ↔ upper with its ($\Delta K = \pm 1$, $\Delta m_J = \pm 2$) matrix elements. By applying a small magnetic field B of ≈2 mT, these hybrid anticrossings are reduced to two separate "two-level" problems: a pure Stark anticrossing that is insensitive to B and a pure hyperfine anticrossing that can have many magnetic components (see section 5.2), each shifted well away from the ($B = 0$) position. While the initial search for these avoided crossings was made in the Earth's field, all the precision crossing field measurements were made with $B \approx 2$ mT on the Stark component only. A full discussion of Stark–hyperfine hybrids is given in ref. [3].

The energy level scheme for the ($J = 2$) member of the ($K = \pm 2 \leftrightarrow \mp 1$) series with $m_J = \pm 2$ is shown in fig. 1. The heavy dots mark the three possible ($\Delta\sigma = 0$) anticrossings, all of which were observed. The unmarked intersections correspond to the ($\Delta\sigma = \pm 1$) anticrossings. The two at lowest field and the two at highest field were searched for and could not be detected. For the remaining two, the search was done on the corresponding series with $m_J = \pm 1$; again they could not be detected. Thus all six of the unmarked intersections in fig. 1 are thought to correspond to forbidden avoided crossings.

The energy level scheme for ($J = 3, K = \pm 3 \leftrightarrow 0$) is very similar to that shown in fig. 2. Of course, the energy levels have to be relabelled; in order of decreasing zero-field energy, these are $(J, K, \sigma, \Gamma) = (3, \pm 3, \mp 1, E_4) \equiv \alpha_1$; $(3, \pm 3, \pm 1, E_4) \equiv \alpha_2$; $(3, \pm 3, 0, A_1 + A_2) \equiv \alpha_3$; $(3, 0, \pm 1, E_4) \equiv \beta_1$; $(3, 0, 0, A_2) \equiv \beta_2$.

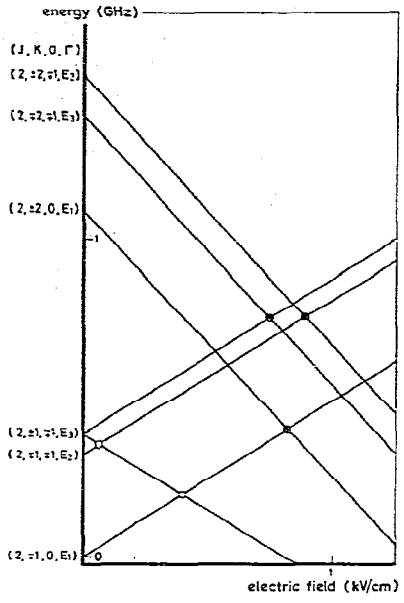

Fig. 1. Schematic plot against the electric field of the energy levels of the $(J, K) = (2, \pm 2)$ and $(2, \mp 1)$ states for $m_J = \pm 2$. Upper signs go with upper and lower with lower. The heavy and open dots indicate the Stark and barrier anticrossings, respectively. For clarity, the torsional splittings have been enlarged slightly.

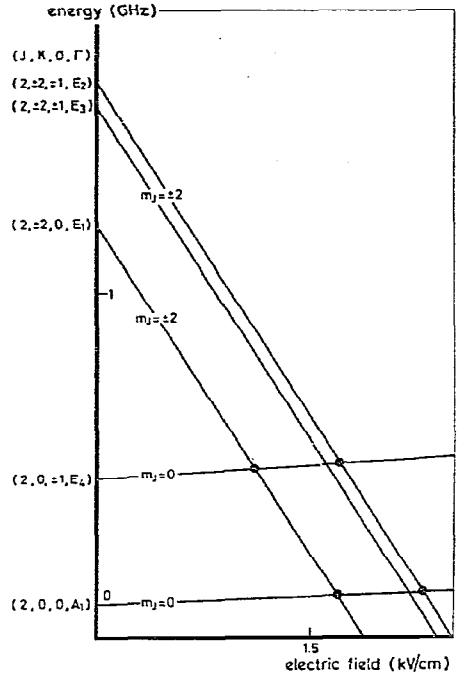

Fig. 2. Schematic plot against the electric field of the energy levels of the $(J, K) = (2, \pm 2)$ and $(2, 0)$ states. For clarity, the quadratic Stark effect of the $(K = 0)$ state has been exaggerated and the torsional splittings have been enlarged slightly. The dots indicate the observed hyperfine rotational anticrossings.

In this case, the $(\Delta\sigma = \pm 1)$ anticrossings were not searched for. However, as specified in table 2, the $(\Delta\sigma = 0)$ anticrossings were observed: $\alpha_1 \leftrightarrow \beta_1$; $\alpha_2 \leftrightarrow \beta_1$; $\alpha_3 \leftrightarrow \beta_2$. In the last case, if we adopt the more restrictive $(\Delta\Gamma = 0)$ form of the selection rule, only the A_2 sublevels in α_3 can interact with β_2, as is indicated in table 2.

The typical anticrossing spectrum consisted of a single line at a frequency ≈1 MHz with the electric field slightly above or below ϵ_c. The values of ϵ_c were ≈8.5 kV/cm for the $(K = \pm 3 \leftrightarrow 0)$ series and the member of the $(K = \pm 2 \leftrightarrow \mp 1)$ series with $J = 5$ and $m_J = \pm 1$. The values of ϵ_c for the other members of the $(K = \pm 2 \leftrightarrow \mp 1)$ series were ≈1.5 kV/cm. As indicated in section 4, different C-fields were used in the two cases. The values of $\Delta\nu_T$ were ≈33 kHz and ≈14 kHz for the higher and lower field cases, respectively. In each case, $\Delta\nu_{obs}$ was broadened by field inhomogeneities of ≈14 ppm. The signal-to-noise for a single sweep at a time constant of 1 s ranged from 0.5 to 6.

For most runs, the spectra were taken with a signal-averager; sufficient scans were taken to build the signal-to-noise up to at least 5/1.

The determination of the zero-field splittings Δ_0 from the crossing field ϵ_c follows from a simple extension of the analysis developed earlier for C_{3v} molecules [3]. For a Stark anticrossing, the value of Δ_0 is independent of magnetic and hyperfine effects. The dipole moment μ is assumed to be constant at the reference value μ_r, which here is taken to be $\mu_Q(3,2)$ as determined in section 4. The rotational dependence of μ as given in eq. (3) is absorbed into Δ_0 to form an apparent zero-field splitting Δ_0^A. The expression for Δ_0^A corresponding to eq. (18) in ref. [3] is here given by:

$$\Delta_0^A = (K_\alpha^2 - K_\beta^2)[a - J(J+1)\,b]\,, \qquad (4a)$$

where

$$a = [(A - B) + (-a_1 F)(2\pi^2\rho^2/9)](1 + \xi) - (K_\alpha^2 - K_\beta^2) D_K , \quad (4b)$$

$$b = D_{JK} + (A - B)\mu_J/\mu_0 - (-a_1^J F)(2\pi^2\rho^2/9) , \quad (4c)$$

$$\xi = J_\tau(J_\tau + 1)\mu_J/\mu_0 + [K_\tau^2 - (K_\alpha^2 - K_\beta^2)]\mu_K/\mu_0 . \quad (4d)$$

K_α and K_β are the K-values for the upper and lower states, respectively. a_1 is the lowest-order coefficient in the Fourier expansion of the pure torsional energy [10]. (a_1 is negative.) a_1^J is the effective J-dependence in a_1 produced by H_D. As can be seen from eq. (2), a_1^J can be expressed in terms of D_{Jm}, F_{3J}, and F_{9J}. For CH_3SiF_3, $-a_1^J F = 0.80(3)$ kHz.

In *absolute* measurements of ϵ_c, the accuracy in determining Δ_0^A is limited to 20 ppm by the long-term stability and resettability of the voltage source for the C-field. However, in *relative* measurements where two different anticrossing spectra are observed in the same field, the error contributed by the voltage source is its short-time stability of 2 ppm. This same error applies when the "splitting method" is used [20], in which the total C-field voltage is changed by $\lesssim 2\%$ with a second voltage source connected to the lower C-field plate.

In *relative* measurements, optimum use can be made of the improved accuracy by taking the piece of data in the fit to be either the difference [3] or the ratio of the two zero-field splittings. If the two linear Stark coefficients are equal, then the difference and ratio are equivalent, although the former is often more easily interpreted. If the two linear Stark coefficients are different, the ratio makes better use of the data; the error in μ_τ cancels in the ratio, but makes a contribution to the difference.

The first step in reducing the data was the determination of b from a relative measurement of the difference in Δ_0^A between two anticrossings with the same linear Stark coefficient, namely $(J, K, \sigma, m_J) = (3, \pm 2, 0, \pm 2) \leftrightarrow (3, \mp 1, 0, \pm 2)$ and $(5, \pm 2, 0, \pm 5) \leftrightarrow (5, \mp 1, 0, \pm 5)$. It was found that $b = 2.700(37)$ kHz. We then determined μ_J from eq. (4c). The value of D_{JK} was taken from the mm-wave spectrum (see section 6). Preliminary values of the reduced barrier height s, ρ, and the various distortion constants entering $-a_1^J F$ were adequate because the term in ρ^2 is very small. The result for μ_J is given in table 1.

The next step was to calculate all the zero-field splittings Δ_0 from the ϵ_c. μ_J was taken into account, but μ_K was neglected. The resulting error becomes significant only if $|\mu_K| > 5|\mu_J|$. In addition, $(\alpha_\parallel - \alpha_\perp)_{eff}$ was neglected. In this case, the error becomes significant only if $|(\alpha_\parallel - \alpha_\perp)_{eff}| \gtrsim 10 \times 10^{-24}$ cm^3. These limits for both $|\mu_K|$ and $|(\alpha_\parallel - \alpha_\perp)_{eff}|$ seem more than adequate for this molecule. The resulting values for Δ_0 are listed in table 3, where Δ_0 is denoted $\nu^S_{\sigma_\alpha,\sigma_\beta}$. The superscript S refers to the mixing mechanism (Stark); the superscript H is used in a similar way for the hyperfine anticrossings. (See section 5.2.) The subscripts σ_α and σ_β indicate the σ-values for the upper level (α) and lower level (β), respectively. The results include eleven absolute measurements, three differences, and one ratio.

The distortion dipole moment μ_D was measured with the method developed for OPF_3 [3] by studying the anticrossing $(J = 4, K = \pm 2, \sigma = 0, m_J = \pm 4) \leftrightarrow (4, \mp 1, 0, \pm 4)$. The relationship between μ_D and the minimum separation ν_m for such a crossing in a C_{3v} molecule [3,6] should apply to CH_3SiF_3:

$$\nu_m = \mu_D \epsilon_c J[(J - 1)(J + 2)]^{1/2} . \quad (5)$$

The applicability of eq. (5) was verified by measurements in CH_3CF_3 where it was shown that the μ_D-values obtained from eq. (5) are independent of J and σ [24]. The present data on CH_3SiF_3 show $\nu_m = (26.5 \pm 7.1)$ kHz and $\mu_D = 2.13(57)$ μD. For comparison, μ_D in OPF_3 is 5.856(20) μD [3].

5.2. The hyperfine rotational anticrossings

A great many different ($\Delta J = 0$) hyperfine anticrossings occur at relatively low field. It was therefore our initial intention to study the selection rules in CH_3SiF_3 just as was done in OPF_3 [3]. By measuring the g-factors of the magnetic components, one can deduce the selection rules on Δm_H and Δm_F, and obtain some insight into the mechanism providing the mixing matrix element η.

A study of this type was carried out for the series of anticrossings $(J = 2, K = \pm 2, \sigma_\alpha, m_J = \pm 2) \leftrightarrow (2, 0, \sigma_\beta, 0)$. The energy level scheme with $B = 0$ is shown in fig. 2. Of the six possible anticrossings, the two involving the upper level with $\Gamma = E_3$ were found to be forbidden. For each of the four detected avoided cros-

Table 3
Zero-field splittings Δ_0 for CH_3SiF_3 in the ground torsional state [a]

J	Upper state			Lower state			Observed value	Observed − calculated	Label
	K_α	σ_α	Γ_α	K_β	σ_β	Γ_β			
2	± 2	0	E_1	∓ 1	0	E_1	1025.287(20)	0.002	$\nu^S_{0,0}$
2	± 2	∓ 1	E_2	∓ 1	∓ 1	E_2	1050.831(20)	−0.003	$\nu^S_{\mp1,\mp1}$
2	± 2	± 1	E_3	∓ 1	± 1	E_3	997.251(20)	0.002	$\nu^S_{\pm1,\pm1}$
3	± 2	0	E_1	∓ 1	0	E_1	1025.237(20)	−0.003	$\nu^S_{0,0}$
3	± 2	∓ 1	E_2	∓ 1	∓ 1	E_2	1050.786(20)	−0.003	$\nu^S_{\mp1,\mp1}$
3	± 2	± 1	E_3	∓ 1	± 1	E_3	997.205(20)	0.002	$\nu^S_{\pm1,\pm1}$
5	± 2	0	E_1	∓ 1	0	E_1	1025.104(20)	0.000	$\nu^S_{0,0}$
5	± 2	∓ 1	E_2	∓ 1	∓ 1	E_2	1050.650(20)	−0.005	$\nu^S_{\mp1,\mp1}$
3	± 3	0	A_2	0	0	A_2	3075.860(62)	−0.012	$\nu^S_{0,0}$
3	± 3	∓ 1	E_4	0	∓ 1	E_4	3098.841(62)	−0.019	$\nu^S_{\mp1,\mp1}$
3	± 3	± 1	E_4	0	± 1	E_4	3045.424(62)	−0.005	$\nu^S_{\pm1,\pm1}$
	$\nu^S_{0,0}(J=2) - \nu^S_{\pm1,\pm1}(J=3)$ [b]						28.0813(30)	0.0006	relative
	$\nu^S_{\mp1,\mp1}(J=2) - \nu^S_{0,0}(J=3)$ [b]						25.5936(25)	0.0007	relative
	$\nu^S_{\mp1,\mp1}(J=3) - \nu^S_{0,0}(J=3)$ [c]						22.9816(85)	−0.0071	relative
	$\nu^S_{0,0}(J=3) - \nu^S_{\pm1,\pm1}(J=3)$ [c]						30.4358(65)	−0.0067	relative
	$\nu^S_{0,0}(J=3)/\nu^S_{\mp1,\mp1}(J=5)$ [d]						2.927577(11)	0.0000018	relative
2	± 2	∓ 1	E_2	0	0	A_1	1673.639(33)	0.000	$\nu^H_{\pm1,0}$
2	± 2	0	E_1	0	± 1	E_4	1076.620(20)	0.006	$\nu^H_{0,\pm1}$
2	± 2	0	E_1	0	0	A_1	1367.041(27)	0.012	$\nu^H_{0,0}$
2	± 2	∓ 1	E_2	0	∓ 1	E_4	1383.228(27)	0.003	$\nu^H_{\mp1,\mp1}$
1	± 1	∓ 1	E_3	∓ 1	0	E_1	298.9336(60)	−0.0008	ν_{EA}
2	± 1	∓ 1	E_3	∓ 1	0	E_1	298.9401(60)	0.0005	ν_{EA}
3	± 1	∓ 1	E_3	∓ 1	0	E_1	298.9496(60)	0.0021	ν_{EA}
5	± 1	∓ 1	E_3	∓ 1	0	E_1	298.9697(60)	−0.0013	ν_{EA}
	$\nu_{EA}(J=2) - \nu_{EA}(J=5)$						−0.0299(12)	0.0016	relative
3	± 1	∓ 1	E_3	∓ 1	∓ 1	E_2	17.87940(40)	0.00012	ν_{EE}
4	± 1	∓ 1	E_3	∓ 1	∓ 1	E_2	17.87990(40)	0.00000	ν_{EE}

[a] All values are in MHz, except the ratio.
[b] Both anticrossings are from the ($K = \pm 2 \leftrightarrow \mp 1$) series.
[c] Both anticrossings are from the ($K = \pm 3 \leftrightarrow 0$) series.
[d] The ($J = 3$) and ($J = 5$) anticrossings are from the ($K = \pm 3 \leftrightarrow 0$) and ($K = \pm 2 \leftrightarrow \mp 1$) series, respectively.

sings, the spectra were comparable in strength and width to the weaker of the low-field Stark anticrossings. The four crossing fields were measured in the Earth's magnetic field. The resulting zero-field splittings Δ_0 are listed as $\nu^{H}_{\sigma_\alpha,\sigma_\beta}$ in table 3, using the notation introduced in section 5.1. Unlike the $\nu^{S}_{\sigma_\alpha,\sigma_\beta}$, these $\nu^{H}_{\sigma_\alpha,\sigma_\beta}$ can contain a contribution from the hyperfine effects [3]. However, the contribution can be neglected since it is small compared to the ≈25 kHz error arising from the calibration of ϵ.

A magnetic field of ≈0.8 T was then applied to determine its effects on the $(\sigma_\alpha = \mp 1) \leftrightarrow (\sigma_\beta = 0)$ member of this series. Since $\Delta m_\Gamma = 0$ and $\Delta m_J = \pm 2$, the spectrum can, a priori, consist of as many as three pairs of magnetic components with selection rules $(\Delta m_H = 0, \Delta m_F = \mp 2)$, $(\Delta m_H = \mp 1, \Delta m_F = \mp 1)$, and $(\Delta m_H = \mp 2, \Delta m_F = 0)$. The corresponding g-factor g_{eff} for each magnetic component in the pair is dominated [3] by the nuclear contribution $\tilde{g} \equiv g_H \Delta m_H + g_F \Delta m_F$, where g_H and g_F are the hydrogen and fluorine g-factors, respectively. Only the magnetic pair with $|\tilde{g}| = 2g_H$ could be detected. The mixing in this case must therefore be due to a tensor of second rank in I_H, most probably the spin–spin interaction between protons. As is discussed in section 7, a careful measurement of g_{eff} was used to determine the absolute sign of the rotational g-factor.

A survey with $(B = 0)$ of other hyperfine avoided crossings was then attempted. For each of the four observed $(\Delta m_J = \pm 2)$ anticrossings discussed above, the corresponding $(\Delta m_J = \pm 1)$ anticrossings were detected. However, the signal-to-noise was significantly lower. It became clear that the experimental work should be preceded by a theoretical investigation of the symmetry properties of the hyperfine hamiltonian under the G_{18} group. This work (currently underway) should predict the selection rules and mixing mechanisms, as was done for C_{3v} molecules [3]. The resulting estimate for η would be very helpful in the experimental search.

Table 2 lists all the hyperfine anticrossings for which searches were made. The major conclusions are that Δm_J can be ± 1 or ± 2 and that the torsion–rotation symmetry can change; the same selection rules were obtained [2] for CH_3CF_3.

5.3. The barrier anticrossings

In the recent work on methyl silane [4], it was shown that the barrier anticrossings form a series between upper level $(\alpha) \equiv (J, K = \pm 1, \sigma_\alpha, \Gamma_\alpha, m_J^\alpha)$ and lower level $(\beta) \equiv (J, K = \mp 1, \sigma_\beta, \Gamma_\beta, m_J^\beta)$ with selection rules $\Delta\sigma = 0, \pm 1$ and $\Delta m_J = 0, \pm 1, \mp 1, \pm 2, \mp 2$. A typical energy level scheme is illustrated in fig. 1. For each J, there are, a priori, three possible anticrossings. Only two could be detected: these (shown in fig. 1) have $\Gamma = E_3 \leftrightarrow E_2$ and $\Gamma = E_3 \leftrightarrow E_1$. The third could not be detected: this (not shown in fig. 1) has $\Gamma = E_2 \leftrightarrow E_1$ and was concluded to be forbidden. The mixing matrix element η is clearly due to the nuclear hyperfine effects. It was suggested that η is dominated by the dipolar interaction between protons.

To see whether these same conclusion can be drawn for methyltrifluorosilane, a survey with $B = 0$ was carried out here of various barrier avoided crossings. The results are summarized in table 2. For convenience, the anticrossings are often referred to by their change in *torsional* symmetry. Thus the $(\Delta\sigma = \pm 1)$ and $(\Delta\sigma = 0)$ cases are referred to as EA and EE anticrossings, respectively.

The major CH_3SiH_3 conclusions were confirmed. Searches for avoided crossings with $K = \pm 2 \leftrightarrow \pm 2$ failed, indicating that, if the energy of rigid rotation is to be conserved in the anticrossing, then $|K_\alpha| = |K_\beta| = 1$. Searches for avoided crossings with $\Gamma = E_2 \leftrightarrow E_1$ failed for both $\Delta m_J = 0$ (as checked in CH_3SiH_3) and $\Delta m_J = \pm 2$ (not previously checked). Again, it is concluded that $\Gamma = E_2 \leftrightarrow E_1$ is forbidden.

The evidence regarding the role of the spin–spin interaction is mixed. On the one hand, as was the case in CH_3SiH_3, the search for the $(J = 3, m_J = \pm 2 \leftrightarrow \pm 2)$ EA member of the series failed, while all similar $(\Delta m_J = 0)$ searches with different (J, m_J) were successful. Because the factor $[3m_J^2 - J(J+1)]$ appears in all dipolar η with $\Delta m_J = 0$, this suggests the dipolar mechanism is dominant. On the other hand, the searches for $(J = 2$, EA) anticrossings were successful for $(m_J = \pm 2 \leftrightarrow \pm 2)$ and $(m_J = \pm 2 \leftrightarrow \pm 1)$, but failed for $(m_J = \pm 2 \leftrightarrow 0)$. This suggests that the dipolar interaction is not dominant for $J = 2$. It should be noted that the $(m_J = \pm 2 \leftrightarrow 0)$ avoided crossing *was* observed in CH_3SiH_3.

To obtain further insight into this problem, a magnetic study of the type described in section 5.2 was

made for the ($J = 2$, EA) anticrossing with ($m_J = \pm 2 \leftrightarrow \pm 1$). A priori, since ($\Delta m_J = \pm 1$), two parts of magnetic components can exist, corresponding to ($\Delta m_H = \mp 1$, $\Delta m_F = 0$) and ($\Delta m_H = 0$, $\Delta m_F = \mp 1$). Only the former components with $\tilde{g} = g_H$ could be found. This indicates that an interaction involving the off-axis spins in the top is operative. In CH_3SiH_3, because both top and frame have the same type of off-axis nuclei, this kind of information distinguishing top and frame interactions cannot be obtained.

The difficulty in interpreting null results should be emphasized, particularly where no systematic pattern has been identified. Conclusions based on such results should be regarded as tentative until their theoretical basis has been established.

Absolute crossing-field measurements were made for six barrier anticrossings. In addition, a relative measurement was made of ϵ_c between the ($J = 5$) and ($J = 2$) EA avoided crossings. The resulting zero-field splittings Δ_0 are listed in table 3 as ν_{EE} and ν_{EA} for the ($\Delta\sigma = 0$) and ($\Delta\sigma = \pm 1$) cases, respectively. All these precision measurements were made on ($\Delta m_J = 0$) anticrossings. In such cases, Δ_0 depends [4] only on the torsional splitting and $\mu_Q(J, K = \pm 1)$ as defined in eq. (3); these avoided crossings are therefore very well suited to precision studies of H_{TR}.

The spectra used to measure the Δ_0 were very similar to those obtained for the rotational anticrossings. The EE crossing fields were $\leqslant 150$ V/cm while the EA crossing fields fell in the range 250–800 V/cm. The value of $\Delta\nu_T$ was ≈ 7 kHz. The observed line widths $\Delta\nu_{obs}$ approach this for the lowest ϵ_c, but were a little larger for the higher ϵ_c.

6. The rotational transitions

The allowed pure rotational spectrum follows the selection rules $(v, J+1, K, \sigma) \leftarrow (v, J, K, \sigma)$. The frequencies $\nu(v, J, K, \sigma)$ can be calculated from eqs. (1) and (2); the only change from the standard expression is the introduction of an effective B-value:

$$\tilde{B}(v, K, \sigma) = B - D_{Jm}\langle p^2\rangle_{vK\sigma} + F_{3J}\langle\tfrac{1}{2}(1 - \cos 3\alpha)\rangle_{vK\sigma} + F_{9J}\langle\tfrac{1}{2}(1 - \cos 9\alpha)\rangle_{vK\sigma} . \quad (6)$$

Here $\langle\Omega\rangle_{vK\sigma}$ represents the diagonal matrix element of operator Ω in the representation which diagonalizes the leading torsional terms in eq. (1). This representation is defined in detail in the discussion of eq. (9) of ref. [4]. It is the (v, K, σ)-variation of B that forms the basis of the torsional satellite method [9].

The microwave spectrum has most recently been investigated by Durig et al. [13]. Frequencies were reported for $1 \leqslant J \leqslant 4$ and $0 \leqslant v \leqslant 3$. The errors quoted for $v = 0$ are 40 kHz; no errors were specified for $v > 0$. The measurements along with the errors assumed here are listed in tables 4 and 5 for $v \leqslant 2$ and $v = 3$, respectively. For $v = 0$ and 1, no splittings were observed. Since a Stark-modulated spectrometer was used, it can be assumed that the ($K = 0$) component did not contribute significantly. The observed frequency is then the average of $\nu(v, J, K, \sigma)$ over the remaining (K, σ) weighted by the corresponding intensities. In view of this averaging, the errors for $v = 0$ and 1 were taken as 100 and 200 kHz, respectively. For $v = 2$ and 3, the σ-splitting was resolved, but not the K-splitting. In this case the K-averaging is done separately for ($\sigma = 0$) and ($\sigma = \pm 1$). Because less averaging is required for each line, the errors were reduced to 150 kHz.

The data set for the pure rotational transitions was extended by studying the ground-state spectra for $J = 13 \leftarrow 12$ and $14 \leftarrow 13$ with a saturation-modulation mm-wave spectrometer [25] and for $J = 1 \leftarrow 0$ with the MBER method [4]. For the mm-wave spectra, the K-splitting was resolved. In all cases, the σ-splitting could not be resolved. Each observed frequency is then the average of $\nu(0, J, K, \sigma)$ over σ. The measurements are listed in table 4.

7. The rotational g-factors

The Zeeman effect on the normal MBER spectrum was studied to obtain $g_\parallel$ and $g_\perp$, the molecular g-factors for rotation, respectively, parallel and perpendicular to the molecular symmetry axis. The techniques used are treated in detail elsewhere [16,19,3]. When a large magnetic field B is applied parallel to $\mathcal{E}$, each Stark multiplet (see section 4) splits into two lines separated by $2\mu_N B|g(J, K)|$, where

$$g(J, K) = g_\perp + (g_\parallel - g_\perp)K^2/J(J+1) . \quad (7)$$

Effects due to nuclear shielding and internal rotation

Table 4
Pure rotational frequencies for CH_3SiF_3 for $v = 0$, 1, and 2 [a]

v	Upper state			Lower state			Observed value	Observed − calculated	Average over [b]
	J_α	K_α	σ_α	J_β	K_β	σ_β			
0	1	0		0	0		7 431.323(15)	0.006	σ
0	2			1			14 862.54(10)	−0.07	K, σ
1	2			1			14 844.72(20)	−0.30	K, σ
2	2		0	1		0	14 828.45(15)	0.18	K
2	2		± 1	1		± 1	14 829.49(15)	−0.11	K
0	3			2			22 293.86(10)	0.02	K, σ
1	3			2			22 267.49(20)	0.03	K, σ
2	3		0	2		0	22 242.30(15)	−0.04	K
2	3		± 1	2		± 1	22 244.38(15)	0.02	K
0	4			3			29 725.02(10)	0.03	K, σ
1	4			3			29 689.87(20)	0.03	K, σ
2	4		0	3		0	29 656.55(15)	0.23	K
2	4		± 1	3		± 1	29 659.06(15)	0.03	K
0	5			4			37 156.13(10)	0.10	K, σ
1	5			4			37 112.17(20)	0.07	K, σ
2	5		0	4		0	37 069.92(15)	−0.28	K
2	5		± 1	4		± 1	37 073.62(15)	0.06	K
0	13	± 5		12	± 5		96 597.995(50)	−0.020	σ
0	13	± 6		12	± 6		96 597.278(50)	−0.007	σ
0	13	± 7		12	± 7		96 596.435(50)	−0.005	σ
0	13	± 8		12	± 8		96 595.445(50)	−0.015	σ
0	13	± 9		12	± 9		96 594.343(50)	0.007	σ
0	13	± 10		12	± 10		96 593.100(50)	0.004	σ
0	13	± 11		12	± 11		96 591.725(50)	0.001	σ
0	13	± 12		12	± 12		96 590.185(50)	−0.022	σ
0	14	± 3		13	± 3		111 457.568(100)	0.000	σ
0	14	± 4		13	± 4		111 457.042(50)	−0.007	σ
0	14	± 5		13	± 5		111 456.364(50)	−0.006	σ
0	14	± 6		13	± 6		111 455.527(50)	0.000	σ
0	14	± 7		13	± 7		111 454.569(50)	0.017	σ
0	14	± 8		13	± 8		111 453.428(50)	0.007	σ
0	14	± 9		13	± 9		111 452.133(50)	0.008	σ
0	14	± 10		13	± 10		111 450.707(50)	0.012	σ
0	14	± 11		13	± 11		111 449.116(50)	0.005	σ

[a] All values are in MHz. The microwave frequencies between 14 and 40 GHz are taken from Durig et al. [13]. The mm-wave frequencies and the $J = 1 \leftarrow 0$ transition were measured in the current work.

[b] The splittings associated with the quantum numbers listed were not resolved. The frequencies listed therefore represent an average over these quantum numbers, with $K = 0$ being excluded from the Stark-modulated data (i.e. the results taken from ref. [13]).

are negligible here. No attempt was made to determine the anisotropy in the magnetic susceptibility.

From Zeeman splittings measured for $B = 819.93(17)$ mT, it was determined that $|g(1,0)| = 0.0178(2)$; $|g(3,\pm 2)| = 0.0202(2)$ and $|g(3,\pm 3)| = 0.0234(3)$, all in units of the nuclear magneton μ_N. From three different $|g(J,K)|$, we determined the magnitudes of $g_\parallel$ and $g_\perp$, as well as showing that $g_\parallel/g_\perp > 0$.

The absolute signs of the g-factors were obtained by the anticrossing method [3] using the hyperfine rotational avoided crossing ($J = 2, K = \pm 2, \sigma = \mp 1$, $m_J = \pm 2$) $\leftrightarrow$ (2,0,0,0). As discussed in section 5.2, this anticrossing spectrum splits into two components. As with the allowed spectrum, the separation is given by $2\mu_N B$ times an effective g-factor g_{eff}. In this case, however [3],

Table 5
Pure rotational frequencies for CH_3SiF_3 for $v = 3$ a)

J b)	Torsional symmetry	Observed value	Predicted value	δ c)	$\delta/(J+1)$
1	A	14 813.84(15)	14 818.07(13)	−4.23(14)	−2.12
2	A	22 220.73(15)	22 227.00(21)	−6.27(21)	−2.09
3	A	29 627.67(15)	29 635.74(28)	−8.07(27)	−2.02
4	A	37 034.58(15)	37 044.40(35)	−9.82(34)	−1.96
1	E	14 810.56(15)	14 813.53(11)	−2.97(11)	−1.49
2	E	22 215.52(15)	22 220.19(17)	−4.67(16)	−1.56
3	E	29.620.81 (15)	29.626.79(23)	−5.98(22)	−1.50
4	E	37 025.49(15)	37 033.32(28)	−7.83(27)	−1.57

a) All values are in MHz. The observed frequencies are taken from Durig et al. [13], along with the assignment, here referred to as #1. In an alternative (albeit speculative) identification, here referred to as #2, the upper four observed frequencies are assigned to the corresponding E lines.
b) This refers to the lower level in the $(J+1 \leftarrow J)$ transition.
c) $\delta \equiv$ (observed−predicted).

$$g_{\mathrm{eff}} = 2g_{\mathrm{H}} - 2g(2, \pm 2)\,. \tag{8}$$

From measurements made with $B = 800.55(17)$ mT and the known value of g_{H} [26], it was determined that $g(2, \pm 2) = -0.0252(30)$ nm, showing that both g-factors are negative. With the magnitudes and relative signs of $g_{\parallel}$ and $g_{\perp}$ determined from the normal spectrum, it follows from eq. (7) that $|g(2, \pm 2)| = 0.0227(4)$. The good agreement between the two magnitudes provides a stringent test for the data. The final values for $g_{\parallel}$ and $g_{\perp}$ are given in table 1.

8. Analysis and discussion

A simultaneous analysis of the anticrossing splittings in table 3 ($v = 0$) and the rotational frequencies in table 4 ($v \leqslant 2$) was carried out in an attempt to determine A, B, ρ, V_3 and the various distortion constants. The ($v = 3$) data in table 5 are discussed below. The method of analysis and its results closely parallel those for CH_3SiH_3 [4,7].

The anticrossing splittings provide essentially six pieces of information. A value of ρ is obtained with is independent of the other parameters in eqs. (1) and (2) except through a small correction term that is a function only of the reduced barrier height s [7]. Since ρ can be obtained directly from the ratio $\nu_{\mathrm{EA}}(J=3)/\nu_{\mathrm{EE}}(J=3)$, ρ is also highly insensitive to the uncertainties in the dipole moment. The second piece of information is a very accurate value of s itself, determined directly from energy splittings rather than from wavefunctions as in the torsional satellite method.

Three linear combinations of A, D_K, D_{Km}, and F_{3K} are obtained by combining measurements from three types of anticrossings: barrier, Stark rotation with $(K = \pm 2 \leftrightarrow \mp 1)$ and Stark rotation with $(K = \pm 3 \leftrightarrow 0)$. The hyperfine rotational avoided crossings $(K = \pm 2 \leftrightarrow 0)$ do not break the correlations. Because the term in D_K goes as K^4, it can be separated from the others; the most important measurement in this regard is the relative measurement (ratio) of a $(J = 3, K = \pm 3 \leftrightarrow 0)$ anticrossing with a $(J = 5, K = \pm 2 \leftrightarrow \mp 1)$ anticrossing. The terms associated with A, D_{Km}, and F_{3K} all go as K^2. These three constants cannot be isolated; instead, two effective parameters are determined [4,7]:

$$A^{\mathrm{eff}} = A - D_{Km}\,\overline{\langle p^2\rangle_0} + F_{3K}\,\overline{\langle \tfrac{1}{2}(1-\cos 3\alpha)\rangle_0}\,, \tag{9a}$$

$$D_{Km}^{\mathrm{eff}} = D_{Km} + \lambda F_{3K}\,. \tag{9b}$$

Here $\overline{\langle \boldsymbol{\Omega}\rangle}_{v=0}$ is the unweighted average over σ of the diagonal matrix elements $\langle \boldsymbol{\Omega}\rangle_{v=0,K,\sigma}$ of operator $\boldsymbol{\Omega}$. For $v = 0$, this average is independent of K to an accuracy much higher than necessary [7]. λ is a numerical factor whose value for CH_3SiF_3 is 0.01099. Its definition in terms of the matrix elements $\langle p^2\rangle_{v=0,K,\sigma}$ and $\langle \tfrac{1}{2}(1-\cos 3\alpha)\rangle_{v=0,K,\sigma}$ is given in ref. [7].

The value of V_3 is obtained from s using $s \equiv \frac{4}{9} V_3/F$.

F is not a free parameter, but is calculated from $A/\rho(1-\rho)$. Since only A^{eff} is known, it follows that the value obtained for the barrier height is also an effective parameter:

$$V_3^{\mathrm{eff}} = \tfrac{9}{4} s A^{\mathrm{eff}}/\rho(1-\rho) . \qquad (9c)$$

The last piece of information obtained from the anticrossings data is the J-dependence of the torsional splittings, which is determined by F_{3J}, F_{9J}, and D_{Jm}. However, the rotational frequencies are more sensitive to these constants. The main impact of the beam data in this regard is to require the introduction of F_{9J}. If F_{9J} is fixed at zero, then the J-dependence of the anticrossing data is inconsistent with the rotational spectrum. The introduction of either F_{6J} or F_{9J} removes this difficulty, with the latter providing a slightly better fit. In CH_3SiH_3, the F_{9J} fit was also superior. In that case, the improvement was striking [4], leading us to prefer the F_{9J} fit in the current work.

The parameters obtained from the least-squares fit to the ($v \leqslant 2$) data are listed in table 1. The differences between the observed and calculated frequencies are given in tables 3 and 4; the χ^2 for the best fit is 14. The overall agreement is excellent. If F_{6J} is used instead of F_{9J}, the major differences are small changes in four parameters: 30 kHz in B and A, 6 kHz in D_{Jm} and 650 kHz in F_{3J}. Various constants have been omitted from eq. (2) that are of the same order as those retained. See eq. (6) of ref. [4]. None of these was determinable.

In table 5 the frequencies predicted for $v = 3$ with the best-fit parameters of table 1 are compared to the experimental measurements using the original assignment [11,13], here referred to as #1. The differences are larger than the errors by a factor of over 25 and are closely proportional to $(J+1)$. An alternative identification, here referred to as #2, is suggested by table 5. The four upper observed frequencies in table 5 are assigned to the corresponding E lines. The value of $\delta \equiv$ (observed − predicted) is improved dramatically for each of the four lines. However, if this identification is to be adopted, an explanation must be found for the fact that the A lines were not observed [11,13] even though they are expected to be comparable in strength to the E lines. To clarify this point, a Stark-modulated spectrometer was used to reinvestigate the ($J = 5 \leftarrow 4$) spectrum for $v = 3$. No line of suitable intensity could be found in the region predicted for the A line in assignment #2. It must be concluded that the reduction in δ mentioned above were fortuitous and that the original identification is correct.

For identification #1, a satisfactory fit to all the ($v \leqslant 3$) data could not be achieved with torsion–rotation terms previously discussed [4,7,10–12,14]. The torsional energy $E_T(v=3, K, \sigma=0)$ lies only $\approx 4\ \mathrm{cm}^{-1}$ above the top of the barrier, while $E_T(3, K, \pm 1)$ falls below by $\approx 24\ \mathrm{cm}^{-1}$. The A levels would be very sensitive to a small increase in the barrier height, while the E levels would be particularly sensitive to the shape of the potential. The current model may not represent these effects properly. The failure of the fit may also be due to a perturbation of the ($v = 3$) level by a low-lying fundamental. However, the same type of breakdown of the internal rotation model was noted in methyl silane, where the problem of low-lying fundamentals is less severe.

The true values of A and V_3 were obtained, as for CH_3SiH_3 [4], by making two additional fits, one with $D_{Km} \equiv 0$ and the other with $F_{3K} \equiv 0$. From the resulting variation in A and V_3, it was determined that:

$$A = 4059.3 \pm 1.5\ \mathrm{MHz} , \qquad (10a)$$

$$V_3 = 413.97 \pm 0.20\ \mathrm{cm}^{-1} . \qquad (10b)$$

Although the correlation effects have been removed from the results in eq. (10), they will contain contributions from the higher-order terms [7,10,12]. For A, these are expected to be negligible compared to the error, but for V_3 they may be $\approx 1\%$ and hence significant.

The torsional satellite method was used by Kirtman [11] to analyse the ($J = 5 \leftarrow 4$) spectrum of CH_3SiF_3. After conversion [4] to the current notation, his results for the constants in the effective B-value are (in MHz): $B = 3717.86$; $F_{3J} = -19.314$; $D_{Jm} = 0.1105$. No errors were quoted. The value for V_3 was 485(35) cm^{-1}. The agreement with the current results is good, particularly when it is recognized that only three microwave frequencies were used along with assumed values for some of the structural parameters.

With the current results it is possible to do a large part of the r_z structure determination using only symmetric-top data corrected for torsional effects. The value of ρ will deviate from $I_\alpha/(I_\alpha + I_f)$ only through the omission of a small correction term [7], a step which is required by the redundancy relations [7,12].

If this is neglected, then it follows from the values of A and ρ that $I_\alpha = 3.170(2)$ amu Å^2 and $I_f = 121.329(47)$ amu Å^2. The value of I_α obtained for CH_3SiH_3 in a similar manner [4] was 3.165(5) amu Å^2. The close agreement between the two measurements of I_α indicates that the redundancy correction is negligible. From I_α, the distance S_H of the hydrogen atom from the symmetry axis was determined to be 1.0239(3) Å. From I_f, the corresponding distance S_F for the fluorine atom was found to be 1.4590(3) Å.

To pursue the structure further, the moment of inertia I_b for the direction perpendicular to the symmetry axis was calculated for each of three different isotopic species. For the parent species CH_3SiF_3, I_b = 135.926(9) amu Å^2, as obtained directly from B in table 1. For $^{13}CH_3SiF_3$, I_b = 139.392(9) amu Å^2. Here the B-value was calculated from the effective value for the ground state [13] by assuming in eq. (6) that the torsional terms are the same as in the parent species. For CD_3SiF_3, I_b = 152.386(9) amu Å^2. Here B was obtained (along with F_{3J} and D_{Jm}) by refitting the data reported by Kirtman [11]. In the analysis, A and ρ were corrected for the deuteration and then fixed. The remaining parameters were assumed to have the same values as in the parent species.

The structure of the methyl top was then calculated: r_{CH} = 1.0940(6) Å and ∠ HCSi = 110.63(4)°. These are in reasonable agreement with the results of Durig et al.: r_{CH} = 1.081(4) Å and ∠ HCSi = 111.02(50)°; this earlier analysis, of course, used both symmetric- and asymmetric-top data. In the current work, the positions relative to the centre of mass were determined for the carbon atom and the projection of the hydrogen atoms on the symmetry axis. However, the corresponding displacement for the silicon atom could not be obtained because it is too close to the centre of mass.

Acknowledgement

The authors wish to thank Dr. A. Dymanus for many fruitful discussions of this problem, in addition to his continued guidance and inspiration in the field of molecular spectroscopy. The authors would like to thank Dr. P.J.M. Kuijpers for his assistance in obtaining the mm-wave data, and Dr. M. Wong for taking the preliminary microwave spectra around 37 GHz. One of us (IO) wishes to express his appreciation to the National Sciences and Engineering Research Council of Canada for its support. Both authors would like to thank the North Atlantic Treaty Organization Research Grant Program for its assistance through Travel Grant No. 1454.

References

[1] I. Ozier and W.L. Meerts, Phys. Rev. Letters 40 (1978) 226.
[2] W.L. Meerts and I. Ozier, Phys. Rev. Letters 41 (1978) 1109.
[3] I. Ozier and W.L. Meerts, Can. J. Phys. 59 (1981) 150.
[4] W.L. Meerts and I. Ozier, J. Mol. Spectry., to be published.
[5] J.K.G. Watson, J. Mol. Spectry. 40 (1971) 536.
[6] M.R. Aliev and V.M. Mikhaylov, J. Mol. Spectry. 49 (1974) 18.
[7] M. Wong, I. Ozier and W.L. Meerts, in preparation.
[8] E. Hirota, J. Mol. Spectry. 43 (1972) 36.
[9] D. Kivelson, J. Chem. Phys. 22 (1954) 1733; 23 (1955) 2230; 27 (1957) 980.
[10] C.C. Lin and J.D. Swalen, Rev. Mod. Phys. 31 (1959) 841.
[11] B. Kirtman, J. Chem. Phys. 37 (1962) 2516.
[12] R.M. Lees and J.G. Baker, J. Chem. Phys. 48 (1968) 5299.
[13] J.R. Durig, Y.S. Li and C.C. Tong, J. Mol. Struct. 14 (1972) 255.
[14] R.M. Lees, J. Chem. Phys. 59 (1973) 2690.
[15] Y.Y. Kwan and D.M. Dennison, J. Mol. Spectry. 43 (1972) 291.
[16] I. Ozier and W.L. Meerts, J. Mol. Spectry. 93 (1982) 164.
[17] P.R. Bunker, Mol. Phys. 9 (1965) 257.
[18] E.R. Cohen and B.N. Taylor, J. Phys. Chem. Ref. Data 2 (1973) 663.
[19] W.L. Meerts, I. Ozier and A. Dymanus, Can. J. Phys. 57 (1979) 1163.
[20] W.L. Meerts and I. Ozier, J. Chem. Phys. 75 (1981) 596.
[21] F.H. de Leeuw and A. Dymanus, J. Mol. Spectry. 48 (1973) 427;
F.H. de Leeuw, Thesis, Katholieke Universiteit, Nijmegen, The Netherlands (1971).
[22] J.M.L.J. Reinartz and A. Dymanus, Chem. Phys. Letters 24 (1974) 346.
[23] J.K.G. Watson, M. Takami and T. Oka, J. Chem. Phys. 70 (1979) 5376.
[24] W.L. Meerts and I. Ozier, 33rd Symposium on Molecular Spectroscopy, The Ohio State University, Columbus, Ohio, USA, June 12–16, 1978, paper MG6.
[25] P.J.M. Kuijpers, T. Törring and A. Dymanus, Z. Naturforsch. 30a (1975) 1256.
[26] G.H. Fuller, J. Phys. Chem. Ref. Data 5 (1976) 835.